1 **Characteristics and influencing factors of rainfall-induced landslide**
2 **and debris flow hazards in Shaanxi Province, China**

3 Ke Zhang[1*], Sheng Wang[1], Hongjun Bao[2], Xiaomeng Zhao[3]

4 [1]State Key Laboratory of Hydrology-Water Resources and Hydraulic Engineering, and College of Hydrology and Water
5 Resources, Hohai University, Nanjing, Jiangsu, 210098, China
6 [2]National Meteorological Center, China Meteorological Administration, Beijing, 100081, China
7 [3]Shaanxi Climate Center, Xi'an, Shaanxi, 710014, China

8 *Correspondence to*: Ke Zhang (kzhang@hhu.edu.cn)

9 **Abstract** Shaanxi Province, located in Northwest China and spanning multiple hydroclimatic and geological zones, has

10 many areas largely suffering from rainfall-induced landslide and debris flow. The objectives of this study are to reveal the

11 spatiotemporal characteristics of the two hazards and identify their major controlling factors in this region based on a

12 region-wide, comprehensive ground survey-based hazard inventory dataset from 2009-2012. We investigated the

13 spatiotemporal characteristics of the two hazards and quantified the relationships between the occurrence rates of the two

14 hazards and their influencing factors, including antecedent rainfall amount, rainfall duration, rainfall intensity, terrain slope,

15 land cover type and soil type. The results show that landslide has a higher occurrence rate and more extensive distribution

16 than debris flow in this region, while the two hazards are both concentrated in the south with ample rainfall and steep

17 terrains. Both of the hazards show clear seasonalities: July-September for landslide and July for debris flow. Rainfall

18 characteristics (amount, duration and intensity) and slope are the dominant factors controlling slope stability across this

19 region. Debris flow is more sensitive to these rainfall metrics on the high-value ranges than landslide in this region. Land

20 cover is another influencing factor but soil type does not appear to impose consistent impacts on the occurrence of the two

21 hazards. This study not only provides an important inventory data for studying the landslide and debris flow hazards but also

22 add valuable information for modeling and predicting the two hazards to enhance resilience to these hazards in this region.

23 **Keywords** Rainfall-induced landslides; debris flows; spatiotemporal distribution; rainfall intensity; Shaanxi Province; slope

24 stability

25 **1. Introduction**

26 Landslides and debris flows are two widespread and destructive natural hazards around the world (Peruccacci et al.,

27 2012;Huang et al., 2017;Nicolussi et al., 2015;Blothe et al., 2015;Wooten et al., 2008;Hong et al., 2007), which can cause

28 large casualties and economic losses (Jaboyedoff et al., 2012;Hong et al., 2017b;Zhang et al., 2016). Globally, landslides are

29 responsible for approximately 1,000 deaths and about $4 billion property losses per year (Pradhan and Youssef, 2010).

30   Landslide-caused fatalities accounted for 17% of fatalities due to natural hazards (Hong et al., 2015a). For debris flows, it is

31   more difficult to quantify the resultant casualties and damages because it is hard to distinguish debris flow-induced losses

32   with the losses caused by concurrent flood or the other hazards (Borga et al., 2014). China is one of the countries, which are

33   severely affected by geological disasters, including landslide and debris flow (Petley, 2010;Hong et al., 2015a). Statistical

34   report by Chinese Institution of Geological Environmental Monitoring showed that unexpected geological hazards led to

35   1,167 casualties and 6.4 billion CNY property losses per year (Zhang et al., 2017). Another research reported that landslide

36   disasters have caused about 1,100 fatalities and 5~10 billion US dollars in China since 2000 (Hong et al., 2017a).

37   Due to the massive casualties and property damages that the landslide and debris flow may cause, it is essential to have a

38   profound comprehension of the causes, e.g., heavy rainfall, earthquakes and human activities, of these disasters (Chen et al.,

39   2015b). The process of landslide occurrence is a complex non-linear process (Qin et al., 2001;Sorbino et al., 2010) that is

40   influenced by many different factors such as the geological features and hydrological conditions (Zhu et al., 2017). In many

41   regions, rainfall is the primary trigger (Milne et al., 2012) of shallow landslides and debris flows that have posed significant

42   threats to human lives and properties (Gariano et al., 2015;Pradhan and Youssef, 2010). Hence, numerous studies have been

43   conducted on understanding and modeling the rainfall-induced landslides and debris flows.

44   The methods used to predict landslide occurrence can be divided into two general categories, the statistical methods and the

45   physically based models. The representative statistical method is the rainfall threshold methods (Guzzetti et al.,

46   2007;Peruccacci et al., 2012;Gariano et al., 2015;Bogaard and Greco, 2018), which usually builds a simple statistical model

47   quantifying the relationship of landslide occurrence rate or probability with cumulated rainfall (the total rainfall measured

48   from the beginning of the rainfall event to the time of slope failure), rainfall intensity (the average rainfall intensity during

49   the rainfall event), and/or rainfall duration. The physically based models usually use the rainfall time series as the input data

50   to model the slope stability based on the physical processes and mechanisms. There are many physically based landslide

51   forecasting models such as TRIGRS (Baum et al., 2010;Alvioli and Baum, 2016), SHALSTAB (Montgomery and Dietrich,

52   1994), SLIDE (Hong et al., 2015b;Liao et al., 2012), and SLIP (Montrasio and Valentino, 2008). Recently, several studies

53   were conducted to couple the landslide models with distributed hydrological models to develop the coupled flood-landslide

54   models (He et al., 2016;Zhang et al., 2016). Modeling the movement and run-out extent of debris flow is a more complicated

55   process than modeling the slope failure or the landslide occurrence. Numerical simulation of the debris-flow process is

56   usually based on the shallow water equations (Han et al., 2017) and the numerical solutions of the mass and momentum

57   conservation equations using finite element and finite differential methods (Naef et al., 2006;Zhang et al., 2015).

58   Despite various advanced methods and models have been used for the prediction of landslide and debris flow, it is still

59   difficult to completely explain the physical mechanisms controlling slope failure and to accurately predict the occurrence of

60   landslide and debris flow in most areas (Hong et al., 2017a;Althuwaynee et al., 2014). Besides, there are limited efforts on

61   landslide and debris flow prediction in Shaanxi Province, China so far. Additional, most of the previous studies were mainly

62   focused in understanding and modeling landslides and/or debris flows in small and medium-sized areas (Chen et al.,

63   2017;Sun et al., 2016;Chen et al., 2016;Zhuang and Peng, 2014). There is still limited knowledge on the characteristics,

64   distributions, and influencing factors of the landslide and debris flow hazards across this region.

65   Therefore, the objectives of this study are to reveal the spatiotemporal characteristics of rainfall-triggered landslide and

66   debris flow hazards in Shaanxi Province and to identify the major controlling factors of the occurrence of the two hazards.

67   To this end, we firstly compiled an inventory data of rainfall-induced landslides and debris flows events in Shaanxi Province

68   for the period 2009-2012 provided by the geological survey office of Department of Land and Resources of Shaanxi

69   Province. Considering the interannual and intraannual differences in rainfall, we then analyzed the characteristics of

70   spatiotemporal distributions of landslide and debris flow using statistical methods. Next, we derived the characteristics of

71   rainfall processes, terrain slope, land cover type and soil type for each grid cell. Finally, we studied the relationships of

72   landslide and debris flow occurrence rates with rainfall level, terrain slope, land cover type and soil type.

73   2. Study area and data

74   2.1 Description of study area

75   Shaanxi Province, situated in the inland of Northwest China, is located between 105°29′ E-111°15′ E longitude and 31°42′

76   N-39°35′ N latitude with a total area of about 205,800 km². Statistical data show that more than 38 million people live in

77   Shaanxi. Altitude mostly ranges from 350 to 3500 m with a regional average slope of 19.9° (Fig. 1a). In Shaanxi, elevation is

78   higher in the north and south and lower in the middle (Fig. 1a). The average elevation of Qinling Mountains is more than

79   2000 m and it stretches from east to west, representing an important natural line of demarcation between North and South

80   China (Wu and Qian, 2017). The high elevations and relatively steep terrains in many areas of this region make them

81   susceptible to both landslide and debris flow. The Bei Mountains and Qinling Mountains divide Shaanxi Province into three

82   geographical regions: Shaanbei Loess Plateau in the north, Guanzhong Plain (also known as Wei River Basin) in the central

83   area and Qinling-Dabashan Mountains in the south (Jiang et al., 2015). Because of this, land cover shows a distinct regional

84   distribution from north to south: grasslands, cultivated lands and forests (Fig. 1b). The soil type in the study area is mainly

85   loam (Fig. 1c).

86   The hydrological conditions of Shaanxi Province are diverse due to the diversity of its physiographic features and climate,

87   which vary regionally and seasonally. The study area consists of three main climatic zones, semi-arid zone, semi-humid zone

88   and humid zone, distributed from north to south. Regional mean annual temperature is about 6.5-16.6 °C. However,

89   temperature decreases from south to north. Spatial average annual rainfall is 400~600 mm, 500~700 mm and 700~900 mm

90   in northern, central and southern areas, respectively, while precipitation decreases from south to north and is significantly

91   influenced by the mountains. In addition, rainfall has a strong seasonality in this region. Rainfall in summer is the greatest

92   and accounts for 40%-60% of annual rainfall. Rainfall of the remaining seasons decreases in the order of autumn, spring and

93   winter. As rainfall is mostly concentrated in the monsoon season (May-October), rainfall-triggered landslide and debris flow

94   occur frequently during this season.

95   **2.2 Datasets**

96   Data used in this study include rainfall, inventory data of geological hazards, digital elevation model (DEM), land cover, and

97   soil texture data. The rainfall, DEM, land cover and soil texture data are gridded data, while the inventory data of landslide

98   and debris flow hazards is a list of events with recorded locations (latitudes and longitudes), hazard types, causes, occurrence

99   times, and associated casualties.

100   The rainfall data are hourly observations from 756 stations provided by China Meteorological Administration (CMA). We

101   interpolated the site data into gridded data by using the inverse distance weighting method. The spatial resolution of grid is

102   90m. The geological disaster data are from geological survey office of Department of Land and Resources of Shaanxi

103   Province. The DEM data with a spatial resolution of 90m×90m were downloaded from the Geospatial Data Cloud

104   (http://www.gscloud.cn). This database covers land area from 60° N to 60° S and was released to the public in 2003.

105   The GlobeLand30-2010 Product is a product of global land cover at a spatial resolution of 30 m derived from remote sensing

106   images in 2010 (Chen et al., 2015a). The dataset covers land area from 80° N to 80° S and consists of 10 land cover types.

107   These 30 m data were aggregated to the 90-m resolution to match with the DEM data.

108   The soil data is from the Harmonized World Soil Database (HWSD) v1.2 (https://daac.ornl.gov/SOILS/guides/HWSD.html),

109   which were compiled from four source databases, the European Soil Database (ESDB), the 1:1,000,000 soil map of China,

110   various regional SOTER databases (SOTWIS Database), and the Soil Map of the World. The soil database used in the

111   research is classified based on the USDA classification method of soil texture, which includes 13 types. The soil data were

112   also reprojected and resampled to the 90-m resolution.

113   **3. Methodology**

114   To reveal the spatiotemporal distributions of the rainfall-triggered landslide and debris flow hazards, we analyzed the spatial,

115   latitudinal, interannual, and seasonal distributions of these hazard events and the relationship of the number of hazard events

116   with the corresponding rainfall amount.

117   To investigate the impacts of rainfall characteristics, including antecedent rainfall amount (P_a), rainfall duration (D) and

118   rainfall intensity (I), terrain slope (θ), land cover type (L) and soil type (S) on the occurrence rates (R) of the landslide and

119   debris flow, we first projected the locations of these recorded hazard events to the DEM grid with a spatial resolution of 90

120   m. If multiple events of the same type of hazard occurred on the same grid cell within one hour, these events are treated as

121   one event; the earliest occurrence time of these events is treated as the occurrence time of the combined event. From the 90

122   m DEM, we further computed the slope angles for each grid cell. We then tabulated all of the above gridded data with the

123   following attributes: grid cell ID, rainfall event ID, rainfall amount, rainfall duration, rainfall intensity, rain intensity class,

124   slope, land cover type, soil type and hazard type. We defined a rainfall event as an event with continuous rainfall or a

125   combination of several discontinued rains with the non-rain intermittent periods less than or equal to two hours.

126   When we calculated the occurrence rate of one type of hazard, we excluded all grid cells without any reported event of this

127   type of hazard and all rainless events from the analysis. The occurrence rate of a kth type hazard conditional on a given

128   explanatory variable or its class J ($R_{j,k}$) is define as:

129    $$R_{j,k} = \frac{n(J==j \text{ and } K=k)}{n[J==j \text{ and } (K=k \text{ or } K=0)]}$$ (1)

130   where K is the hazard type (0, 1 and 2 for rainfall event without causing any geological hazard, rainfall-induced landslide,

131   rainfall-induce debris flow, respectively); J is the class of P_a, D, I, θ, land cover type and soil type; $n(J == j \text{ and } K = k)$

132   is the number of events of a given hazard k when the corresponding J belongs to the jth class; $n[J == i \text{ and } (K = k \text{ or } K =$

133    $0)]$ is the number of positive and negative events of a given hazard k when the corresponding J belongs to the jth class. In

134   this study, we classified the rainfall amount, rainfall duration, rainfall intensity, and rain type into five (0-10, 10-30, 30-60,

135   60-100, and >100 mm), five (0-3, 3-12, 12-24, 24-36, and >36 hours), five (0-1, 1-2, 2-3, 3-5, >5 mm hour^{-1}), and four

136   classes (light rain, moderate rain, heavy rain, and violent rain), respectively. Following American Meteorology Society

137   (Huschke, 2000), the light rain, moderate rain, heavy rain, and violent rain are defined as rains when the precipitation rate is

138   < 2.5 mm hour^{-1}, 2.5-7.6 mm hour^{-1}, 7.6-50 mm hour^{-1}, and >50 mm hour^{-1}, respectively. We categorized the slope, land

139   cover type and soil type into five (0-2°, 2-5°, 5-10°, 10-20°, and >20°), three (cultivated land, forest, and grassland), and

140   three classes (loamy sand, loam, and clay), respectively. The other land cover types and soil types are not used in the

141   computation of the hazard occurrence rates because we did not find any reported landslide or debris flow event under these

142   types.

143   **4. Results**

144   **4.1 Spatiotemporal distributions of landslide and debris flow events**

145   The locations of the recorded landslide and debris flow events and the resultant casualties from 2009 to 2012 are shown in

146   Fig. 2. It clear that all of these recorded landslide and debris flow events are located in the south of 36° N (Fig. 2).

147   Relatively, debris flow events are distributed further south than landslides. Most of the landslide and debris flow events are

148   near the rivers and/or in the areas with steep slopes (see Fig. 2 and Fig. 1a). In addition, the landslide events outnumber the

149   debris flow events (Fig. 2), indicating that landslide occurs more frequently than debris flow in this region.

150   There are a total of 1177 reported rainfall-triggered landslide events in Shaanxi Province from 2009 to 2012 with respective

151   69, 619, 332 and 157 events in the four years (Fig. 3a), while a total of 209 rainfall-triggered debris flow events occurred in

152   this province during the same period, with respective 6, 175, 13 and 15 events in the four years (Fig. 3a). More than half of

153   the two types of events occurred in 2010. The corresponding casualties are clearly proportional to the number of hazards

154   (Fig. 3a). In particular, landslides and debris flows in 2010 killed 72 and 73 peoples, respectively. During the four-years

155   period, the reported landslide and debris flow hazards caused the deaths of 131 and 78 people, respectively (Fig. 3a),

156   indicating that the two types of hazards are destructive in this region. Relatively, debris flow is even more destructive than

157   landslide. Although the number of debris flow events account for only 15 % of the total events of the two hazards, the debris

158   flow-caused fatalities are 37.32 % of the total deaths caused by the two hazards (Fig. 3b). The above results suggest that

159   debris flow imposes a higher threat to people in this province per event than landslide.

160   In terms of interannual distributions of the two hazards, annual total numbers of landslide and debris flow hazards show a

161   correlation with annual rainfall amount (Fig. 4a). However, annual rainfall amount is not the only factor influencing the

162   occurrences of the two hazards. For example, there is more annual rainfall in 2011 and 2012 than in 2010, but the total

163   numbers of landslide and debris flow events in 2011 and 2012 are actually lower than these in 2010 (Fig. 4a). In terms of

164   intra-annual distributions of the two hazards, landslide events are mainly distributed between July and September, which are

165   the top three months in terms of both total rainfall amount (Fig. 4b) and average rainfall intensity (Fig. 4c). In contrast,

166   almost all of debris flow events occurred in July, the month having the largest rainfall amount (Fig. 4b) and rainfall intensity

167   (Fig. 4c) with multi-year mean values of 117 mm month^{-1} and 0.96 mm hour^{-1}, respectively during a year. Statistical analysis

168   shows that rainfall between July and September accounts for 63.6 % of annual rainfall, while the proportions of landslide

169   and debris flow events during the three months are 98.6 % and 100 % of annual events, respectively. Obviously, the

170   landslide and debris flow hazards are seasonal hazards in Shaanxi Province and mainly occur during the rainy season. The

171   above results show that the landslide season is longer than the debris flow season.

172   We further analyzed the latitudinal distribution of annual rainfall, the number of landslides, the number of debris flows, the

173   zonal average slope, and the percentages of dominant land cover by dividing the region into four latitude bins (31° N-33° N,

174   33° N-34° N, 34° N-35° N and 35° N-36° N). As there are no reported landslide and debris flow events in the areas north to

175   36° N, we excluded these regions for analyzing the distributions of these hazards and their relations to rainfall, terrain slope,

176   and land cover in these areas. There are apparent latitudinal gradients in annual rainfall and the numbers of report landslide

177   and debris flow events, which all decrease from the south to the north (Fig. 5). The regional average terrain slope generally

178   decreases from the south to the north with the respective values of 23.4°, 23.7°, 10.7° and 11.4° in the four latitude bins (Fig.

179   5). These results suggest that more rainfall and steeper slopes in the south can explain the larger numbers of reported

180   landslides and debris flows in the south than in the north. In addition, the southern part of this province (31° N-34° N) is

181   mainly covered by forests (≥78 %), while the regions between 34° N-35° N and between 35° N-36° N are dominated by

182   cultivated lands (50 %) and grasslands (47.1 %), respectively (Fig. 5 and Fig. 1a). Although the southern region has a denser

183   and better preserved land cover than the middle and northern parts, the southern region still experiences more landslide and

184   debris flow hazards. This suggests that the meteorological and geomorphological factors such as rainfall and terrain slope

185   play more important roles in controlling the landslide and debris flow occurrence than land cover.

186   **4.2 Impacts of rainfall amount, intensity, and duration on the landslide and debris flow occurrence**

187   To attribute the causes of the landslide and debris flow hazards, we further analyzed the relationships between rainfall

188   characteristics (antecedent accumulated amount, duration and intensity) and the occurrence rates of the two hazards. There

189   are no apparent relationships between the antecedent rainfall amount and the number of the landslide events and between the

190   antecedent rainfall amount and the number of the debris flow events (Fig. 6a). However, the occurrence rate of debris flow

191   exponentially increases with increasing antecedent rainfall amount ($R = 0.0022\exp(1.8127P_a)$; R^2=0.988) (Fig. 6a).

192   Similar relationship appears between the landslide occurrence rate and antecedent rainfall amount

193   ($R = 0.0034\exp(1.6681P_a)$; R^2=0.977). However, the landslide occurrence rate is higher than the debris flow occurrence

194   rate when antecedent accumulated rainfall is lower than 100 mm (Fig. 6a). Once antecedent accumulated rainfall is above

195   100 mm, the debris flow occurrence rate becomes much larger than the landslide occurrence rate (Fig. 6a). This suggests that

196   triggering debris low generally requires more rainfall than triggering landslide.

197   The occurrence rates of the two hazards also show positive exponential relationships with the rainfall duration ($R = $

198    $0.0002\exp(1.7175D)$, R^2=0.997 for landslide; $R = 0.00009\exp(1.9526D)$, R^2=0.977 for debris flow) (Fig. 6b). In

199   addition, the occurrence rates of the two hazards also show positive exponential relationships with the average rainfall

200   intensity (Fig. 6c). These results indicate that rainfall amount, duration, and intensity all play an important role in controlling

201   the landslide and debris flow occurrence in this region. In addition, the three rainfall metrics usually correlate with each

202   other to some extent. In other words, the rainfall event that has the largest accumulated rainfall usually has a long duration

203   and high average rainfall intensity.

204   In terms of the rainfall intensity, rainfall events can be classified to four classes, i.e., light rain, moderate rain, heavy rain,

205   and violent rain according to American Meteorology Society. Therefore, we also calculated the regional average occurrence

206   rates of landslide and debris flow under the four rain classes. Similar to the relationships between the occurrence rates and

207   rainfall intensity (Fig. 6c), the regional average occurrence rates of the two hazards increase largely with increasing rainfall

208   class (Fig. 7). Furthermore, Fig. 8 shows the spatial maps of landslide and debris occurrence rates under different rain

209   classes. As rain becomes severe, both landslide and debris flow occur on more grid cells (Fig. 8a-d and Fig. 8e-h). For

210   example, light rains have caused 163 landslide events and 26 debris flow events during the four-years period with average

211   occurrence rates of 0.006 % and 0.005 %, respectively. In contrast, violent rains have led to 273 landslide events and 60

212   debris flow events during the same period with average occurrence rates of 2.70 % and 8.57 %, respectively. Meanwhile, the

213   landslide occurrence rates on the grid cells that experience at least one landslide event during the four-years period increase

214   with increased rainfall intensity as well (Fig. 8a-d). As shown in Fig. 8e-h, the debris flow occurrence rates on the grid cells

215   that experience at least one debris flow event during the four-years period show a similar correlation with the rain classes (or

216   rainfall intensity classes).

217   **4.3 Relationship of the landslide and debris flow occurrence with slope, land cover type, and soil type**

218   Terrain, in particular terrain slope, is another important factor determining slope stability. Therefore, we grouped the 90-m

219   grid cells with at least one reported landslide or debris flow event during the study period into five slope bins, i.e., 0-2°, 2-5°,

220   5-10°, 10-20°, and >20°, and computed the respective landslide and debris flow occurrence rates. It is obvious that there are

221   strong positive correlations between the occurrence rates of the two hazards and the slope angle (Fig. 9). Once again, the

222   landslide occurrence rate is clearly larger than the debris flow occurrence rate under all of the five slope classes (Fig. 9).

223   Relative to debris flow, landslide occurrence is more sensitive to terrain slope (Fig. 9). With increasing terrain slope, the

224   landslide occurrence rate accelerates much faster than the debris flow occurrence rate.

225   We further analyzed the relationships of the hazard occurrence rates with land cover type and soil type. For debris flow, its

226   occurrence rate is higher on the cultivated lands, followed by forests and grasslands (Fig. 10a). As shown in Fig. 1b,

227   grasslands are mainly located in the north that has lower rainfall and much flatter terrain than in the south. Therefore, it is not

228   surprise to observe a lower debris flow occurrence rate on grasslands than on cultivated lands and forests. For landslide, its

229   occurrence rate is also the highest on cultivated lands, but the occurrence rates on forests and grasslands are very similar

230   (Fig. 10a). Higher occurrence rates for both landslide and debris flow on cultivated lands than on forests and grassland

231   suggest that the destruction and conversion of natural dense land cover can weaken slope stability, making these areas more

232   susceptible to landslides.

233   In this region, our analysis based on the available data does not show that soil type imposes apparent, consistent effects on

234   the occurrence rates of landslide and debris flow. For example, landslide has the highest occurrence rate in the clay soil

235   among the tree dominant soil types in this region, while the landslide occurrence rates in the loam soil and the loamy sand

236   soil are comparable (Fig. 10b). In contrast, debris flow has the highest occurrence rate in the loamy sand soil, while the

237   debris flow occurrence rates are similar in the loam and clay soils (Fig. 10b).

238   **5. Discussions**

239   Based on the survey of rainfall-induced landslide and debris flow hazards from 2009 to 2012 in Shaanxi Province, China,

240   our results show that both of landslide and debris flow occur frequently in this region and are mainly distributed in the

241   southern part of this province, which have more rainfall and steeper terrain slopes than the other areas of this province.

242   Landslide happens more frequently than debris flow. Although the number of the reported debris flow events is only one

243   sixth of the number of the recorded landslide events in this region, the debris flow-caused casualties is equal to 60 % of the

244   landslide-caused casualties. Clearly, debris flow is more destructive than landslide in this region in terms of the casualty per

245   event. Like many areas in the world, debris flow usually occurs in the areas near the stream network, which usually has

246   higher population. Moreover, debris flow usually carries more materials and travels a longer distance than landslide , making

247   it more harmful to the people and properties(Ietto et al., 2016). In fact, most of debris flow events are initialized from

248   landslide and cause more damages to the environment and society (Peng et al., 2015;Zhou et al., 2013).

249   Our results show that rainfall characteristics including rainfall amount, rainfall intensity, and rainfall duration all play

250   important roles in controlling the occurrence of landslide and debris flow. Relatively speaking, rainfall amount and rainfall

251   duration have higher impacts on the occurrence of landslide and debris flow than average rainfall intensity in this region.

252   This is because a rainstorm with higher average rainfall intensity does not necessary last for a long duration and lead to

253   larger accumulated rainfall amount. In addition, one has to note that the three rainfall characteristics do not necessary

254   correlate with each other. The previous studies have pointed out that different types of landslides and debris flows have

255   different critical rainfall conditions for failure considering the different geologic and geomorphologic conditions (Zezere et

256   al., 2015;Guzzetti et al., 2008). For example, rapid debris flows are typically triggered by very intense showers concentrated

257   in a few hours, while shallow translational soil slips are usually triggered by intense precipitation falling within a few days

258   (Zezere et al., 2015). In contrast, deep-seated landslides of rotational, translational and complex types are related to long

259   periods (weeks to months) of nearly constant rainfall (Zezere et al., 2015;Chen et al., 2013). In general, rainfall with long

260   duration and large rainfall amount is more likely to trigger landslide and debris flow (Saito et al., 2014).

261   Terrain slope is another important factor influencing the slope stability since gravity makes these slopes with higher slope

262   angles more vulnerable (Nourani et al., 2014;Dehnavi et al., 2015). In addition, terrains with steep slopes make plants harder

263   to establish and grow. Furthermore, the vegetation roots are hard to reach the sliding surface if the slope is steep (usually

264   exceed 1.5 m) (Ocakoglu et al., 2002;Cammeraat et al., 2005). In this case vegetation biomass may increase the weight of

265   landslide body and promote the occurrence of landslides (Nilaweera and Nutalaya, 1999;Collison and Anderson, 1996). The

266   terrain and vegetation can interact with each to create complex hydrological and mechanical effects on the slope stability.

267   Benefits from vegetation are conditional on the geological and geomorphological conditions (Nilaweera and Nutalaya,

268   1999;Collison and Anderson, 1996).

269   Land cover type is another factor that impacts the slope stability. As show in our results (Fig. 10), cultivated lands have

270   higher landslide and debris flow occurrence rates than forests in the same climatic zone. The similar findings were also

271   reported in the previous researches, showing that conversion of natural vegetated lands, in particular forests, to cultivated

272   lands or the early-stage abandonment of cultivated lands can largely weaken slope stability by increasing surface water

273   runoff, intensifying erosion processes, and increasing soil instability (Begueria, 2006;Lopez-Saez et al., 2016;Persichillo et

274   al., 2017). Besides, the slopes with woody vegetation are more stable than those with herbaceous vegetation because woody

275   vegetation has deeper roots than herbaceous vegetation and can draw down soil moisture, making the slopes more stable

276   (Kim et al., 2017;Begueria, 2006). In addition, some studies also show that the stand age, structure and composition of

277   vegetation can influence the slope stability (Turner et al., 2010).

278   In this region, soil type does not appear to impose apparent, consistent effects on the occurrence rates of landslide and debris

279   flow based on the available data. These results suggest that soil type is not the dominant factor influencing the slope stability

280   in this region. As shown in the other studies, soil types and their physical properties such as cohesion, saturated hydraulic

281   conductivity, porosity and friction angle have impacts on the slope failure and stability (Antinoro et al., 2017;van Asch and

282   Malet, 2009;Zhang et al., 2016;Pasculli et al., 2017;Milne et al., 2012).

283   **6. Conclusions**

284   In this paper, we analyzed the spatiotemporal distributions, occurrence rates, and resultant casualties of rainfall-triggered

285   landslide and debris flow based on a survey from 2009 to 2012 in Shaanxi Province, China. Our results show that landslide

286   has a higher occurrence rate and more extensive distribution than debris flow in Shaanxi Province, while both of the two

287   hazards are concentrated in the south of this region with ample rainfall and relatively steep terrains. Debris flow is more

288   destructive than landslide in terms of the casualties per event. Both landslide and debris flow show a clear seasonality,

289   corresponding to the rainy season in this region. Debris flow mainly occurs in July, whereas landslide usually takes place

290   between July and September.

291   The characteristics of rainfall events including accumulated rainfall amount, duration and intensity and terrain slope show

292   the strongest impacts on the slope stability and the occurrence rates of landslide and debris flow. The landslide and debris

293   flow occurrences have exponential relationships with all of the above four factors (P < 0.1). When accumulated rainfall

294   amount and intensity are on the low and intermediate levels, landslide has a higher occurrence rate than debris flow. On the

295   contrary, the debris flow occurrence rate is much higher than the landslide occurrence rate when accumulated rainfall

296   amount and intensity are on the high level. Responses of the landslide and debris flow occurrence rates to rainfall duration

297   do not differ much between each other. The occurrence of both landslide and debris flow also largely depends on the terrain

298   slope, but landslide has a higher sensitivity to terrain slope than debris flow does. Our results also show that land cover also

299   influences the occurrence of the two hazards to some extent in this region. In particular, both landslide and debris flow has

300   lower occurrence rates on the natural vegetated land than on the cultivated lands. However, the study does not find an

301   apparent relationship between the occurrence rates of the two hazards and soil type. In summary, we compiled an important

302   inventory data of the rainfall-triggered landslide and debris flow hazards in Shaanxi Province, China based on a four-years

303 survey and revealed the spatiotemporal distributions and characteristics of these events and the impacts of rainfall

304 characteristics, topography and soil texture on the occurrence of landslide and debris. This study not only provides an

305 important inventory data for understanding the formation mechanisms and characteristics of the landslide and debris flow

306 hazards but also add valuable information for modeling and predicting the rainfall-triggered landslide and debris flow

307 hazards to improve preparedness for and enhance resilience to these hazards in this region and the other similar areas.

308 **Author contribution:** K.Z. designed the study; S.W. and K.Z. conducted this study; K.Z. and S.W. wrote this paper; H.B.

309 and X.Z. provided the data and reviewed this paper.

310 **Competing interests:** The authors declare that they have no conflict of interest.

311 **Acknowledgments:** This study was supported by the National Key Research and Development Program of China

312 (2016YFC0402701), National Natural Science Foundation of China (518679067, 51579131, 41875131), Fundamental

313 Research Funds for the Central Universities of China (2015B28514, 2018B42914), Open Foundation of State Key

314 Laboratory of Hydrology-Water Resources and Hydraulic Engineering (20165042212), and Priority Academic Program

315 Development of Jiangsu Higher Education Institutions.

316 **References**

317 Althuwaynee, O. F., Pradhan, B., Park, H. J., and Lee, J. H.: A novel ensemble bivariate statistical evidential belief function
318 with knowledge-based analytical hierarchy process and multivariate statistical logistic regression for landslide susceptibility
319 mapping, Catena, 114, 21-36, 10.1016/j.catena.2013.10.011, 2014.
320 Alvioli, M., and Baum, R. L.: Parallelization of the TRIGRS model for rainfall-induced landslides using the message passing
321 interface, Environmental Modelling & Software, 81, 122-135, 2016.
322 Antinoro, C., Arnone, E., and Noto, L. V.: The use of soil water retention curve models in analyzing slope stability in
323 differently structured soils, Catena, 150, 133-145, 10.1016/j.catena.2016.11.019, 2017.
324 Baum, R. L., Godt, J. W., and Savage, W. Z.: Estimating the timing and location of shallow rainfall-induced landslides using
325 a model for transient, unsaturated infiltration, J. Geophys. Res., 115, F03013, doi: 10.1029/2009jf001321, 2010.
326 Begueria, S.: Changes in land cover and shallow landslide activity: A case study in the Spanish Pyrenees, Geomorphology,
327 74, 196-206, 10.1016/j.geomorph.2005.07.018, 2006.
328 Blothe, J. H., Korup, O., and Schwanghart, W.: Large landslides lie low: Excess topography in the Himalaya-Karakoram
329 ranges, Geology, 43, 523-526, 10.1130/g36527.1, 2015.
330 Bogaard, T., and Greco, R.: Invited perspectives: Hydrological perspectives on precipitation intensity-duration thresholds for
331 landslide initiation: proposing hydro-meteorological thresholds, Nat Hazard Earth Sys, 18, 31-39, 10.5194/nhess-18-31-2018,
332 2018.
333 Borga, M., Stoffel, M., Marchi, L., Marra, F., and Jakob, M.: Hydrogeomorphic response to extreme rainfall in headwater
334 systems: Flash floods and debris flows, J. Hydrol., 518, 194-205, 10.1016/j.jhydrol.2014.05.022, 2014.
335 Cammeraat, E., van Beek, R., and Kooijman, A.: Vegetation succession and its consequences for slope stability in SE Spain,
336 Plant and Soil, 278, 135-147, 10.1007/s11104-005-5893-1, 2005.
337 Chen, J., Chen, J., Liao, A. P., Cao, X., Chen, L. J., Chen, X. H., He, C. Y., Han, G., Peng, S., Lu, M., Zhang, W. W., Tong,
338 X. H., and Mills, J.: Global land cover mapping at 30 m resolution: A POK-based operational approach, Isprs Journal of
339 Photogrammetry and Remote Sensing, 103, 7-27, 2015a.
340 Chen, J. J., Zeng, Z. G., Jiang, P., and Tang, H. M.: Deformation prediction of landslide based on functional network,

341   Neurocomputing, 149, 151-157, 10.1016/j.neucom.2013.10.044, 2015b.

342   Chen, W., Chai, H. C., Zhao, Z., Wang, Q. Q., and Hong, H. Y.: Landslide susceptibility mapping based on GIS and support

343   vector machine models for the Qianyang County, China, Environ Earth Sci, 75, ARTN 474

344   10.1007/s12665-015-5093-0, 2016.

345   Chen, W., Pourghasemi, H. R., and Zhao, Z.: A GIS-based comparative study of Dempster-Shafer, logistic regression and

346   artificial   neural   network   models   for   landslide   susceptibility   mapping,   Geocarto   Int,   32,   367-385,

347   10.1080/10106049.2016.1140824, 2017.

348   Chen, Y. C., Chang, K. T., Chiu, Y. J., Lau, S. M., and Lee, H. Y.: Quantifying rainfall controls on catchment-scale landslide

349   erosion in Taiwan, Earth Surface Processes and Landforms, 38, 372-382, 2013.

350   Collison, A. J. C., and Anderson, M. G.: Using a combined slope hydrology stability model to identify suitable conditions

351   for landslide prevention by vegetation in the humid tropics, Earth Surface Processes and Landforms, 21, 737-747, Doi

352   10.1002/(Sici)1096-9837(199608)21:8<737::Aid-Esp674>3.0.Co;2-F, 1996.

353   Dehnavi, A., Aghdam, I. N., Pradhan, B., and Varzandeh, M. H. M.: A new hybrid model using step-wise weight assessment

354   ratio analysis (SWAM) technique and adaptive neuro-fuzzy inference system (ANFIS) for regional landslide hazard

355   assessment in Iran, Catena, 135, 122-148, 10.1016/j.catena.2015.07.020, 2015.

356   Gariano, S. L., Brunetti, M. T., Iovine, G., Melillo, M., Peruccacci, S., Terranova, O., Vennari, C., and Guzzetti, F.:

357   Calibration and validation of rainfall thresholds for shallow landslide forecasting in Sicily, southern Italy, Geomorphology,

358   228, 653-665, 2015.

359   Guzzetti, F., Peruccacci, S., Rossi, M., and Stark, C. P.: Rainfall thresholds for the initiation of landslides in central and

360   southern Europe, Meteorology and Atmospheric Physics, 98, 239-267, 10.1007/s00703-007-0262-7, 2007.

361   Guzzetti, F., Peruccacci, S., Rossi, M., and Stark, C. P.: The rainfall intensity-duration control of shallow landslides and

362   debris flows: an update, Landslides, 5, 3-17, 10.1007/s10346-007-0112-1, 2008.

363   Han, Z., Li, Y. G., Huang, J. L., Chen, G. Q., Xu, L. R., Tang, C., Zhang, H., and Shang, Y. H.: Numerical simulation for

364   run-out extent of debris flows using an improved cellular automaton model, B Eng Geol Environ, 76, 961-974, 2017.

365   He, X. G., Hong, Y., Vergara, H., Zhang, K., Kirstetter, P. E., Gourley, J. J., Zhang, Y., Qiao, G., and Liu, C.: Development

366   of a coupled hydrological-geotechnical framework for rainfall-induced landslides prediction, J. Hydrol., 543, 395-405, 2016.

367   Hong, H. Y., Pradhan, B., Xu, C., and Tien Bui, D.: Spatial prediction of landslide hazard at the Yihuang area (China) using

368   two-class kernel logistic regression, alternating decision tree and support vector machines, Catena, 133, 266-281,

369   10.1016/j.catena.2015.05.019, 2015a.

370   Hong, H. Y., Chen, W., Xu, C., Youssef, A. M., Pradhan, B., and Bui, D. T.: Rainfall-induced landslide susceptibility

371   assessment at the Chongren area (China) using frequency ratio, certainty factor, and index of entropy, Geocarto Int, 32,

372   139-154, 10.1080/10106049.2015.1130086, 2017a.

373   Hong, H. Y., Liu, J. Z., Zhu, A. X., Shahabi, H., Pham, B. T., Chen, W., Pradhan, B., and Bui, D. T.: A novel hybrid

374   integration model using support vector machines and random subspace for weather-triggered landslide susceptibility

375   assessment in the Wuning area (China), Environ Earth Sci, 76, ARTN 652

376   10.1007/s12665-017-6981-2, 2017b.

377   Hong, Y., Adler, R., and Huffman, G.: Use of satellite remote sensing data in the mapping of global landslide susceptibility,

378   Nat Hazards, 43, 245-256, 2007.

379   Hong, Y., He, X. G., Cerato, A., Zhang, K., Hong, Z., and Liao, Z. H.: Predictability of a Physically Based Model for

380   Rainfall-induced Shallow Landslides: Model Development and Case Studies, Modern Technologies for Landslide

381   Monitoring and Prediction, 165-178, 10.1007/978-3-662-45931-7_9, 2015b.

382   Huang, X. H., Li, Z. Y., Yu, D., Xu, Q., Fan, J. Y., Hao, Z., and Niu, Y. P.: Evolution of a giant debris flow in the

383   transitional mountainous region between the Tibetan Plateau and the Qinling Mountain range, Western China: Constraints

384   from broadband seismic records, J Asian Earth Sci, 148, 181-191, 10.1016/j.jseaes.2017.08.031, 2017.

385   Huschke, R. E.: Glossary of Meteorology, American Meteorological Society, 69-86 pp., 2000.

386   Ietto, F., Perri, F., and Cella, F.: Geotechnical and landslide aspects in weathered granitoid rock masses (Serre Massif,

387   southern Calabria, Italy), Catena, 145, 301-315, 10.1016/j.catena.2016.06.027, 2016.

388 Jaboyedoff, M., Oppikofer, T., Abellan, A., Derron, M. H., Loye, A., Metzger, R., and Pedrazzini, A.: Use of LIDAR in
389 landslide investigations: a review, Nat Hazards, 61, 5-28, 10.1007/s11069-010-9634-2, 2012.
390 Jiang, R. G., Xie, J. C., He, H. L., Luo, J. G., and Zhu, J. W.: Use of four drought indices for evaluating drought
391 characteristics under climate change in Shaanxi, China: 1951-2012, Nat Hazards, 75, 2885-2903,
392 10.1007/s11069-014-1468-x, 2015.
393 Kim, J. H., Fourcaud, T., Jourdan, C., Maeght, J. L., Mao, Z., Metayer, J., Meylan, L., Pierret, A., Rapidel, B., Roupsard, O.,
394 de Rouw, A., Sanchez, M. V., Wang, Y., and Stokes, A.: Vegetation as a driver of temporal variations in slope stability: The
395 impact of hydrological processes, Geophys. Res. Lett., 44, 4897-4907, 10.1002/2017gl073174, 2017.
396 Liao, Z. H., Hong, Y., Kirschbaum, D., and Liu, C.: Assessment of shallow landslides from Hurricane Mitch in central
397 America using a physically based model, Environ Earth Sci, 66, 1697-1705, 10.1007/s12665-011-0997-9, 2012.
398 Lopez-Saez, J., Corona, C., Eckert, N., Stoffel, M., Bourrier, F., and Berger, F.: Impacts of land-use and land-cover changes
399 on rockfall propagation: Insights from the Grenoble conurbation, Sci. Total Environ., 547, 345-355,
400 10.1016/j.scitotenv.2015.12.148, 2016.
401 Milne, F. D., BrownA, M. J., Knappett, J. A., and Davies, M. C. R.: Centrifuge modelling of hillslope debris flow initiation,
402 Catena, 92, 162-171, 2012.
403 Montgomery, D. R., and Dietrich, W. E.: A physically based model for the topographic control on shallow landsliding,
404 Water Resour. Res., 30, 1153–1171, 1994.
405 Montrasio, L., and Valentino, R.: A model for triggering mechanisms of shallow landslides, Nat Hazard Earth Sys, 8,
406 1149-1159, 2008.
407 Naef, D., Rickenmann, D., Rutschmann, P., and McArdell, B. W.: Comparison of flow resistance relations for debris flows
408 using a one-dimensional finite element simulation model, Nat Hazard Earth Sys, 6, 155-165, 2006.
409 Nicolussi, K., Spotl, C., Thurner, A., and Reimer, P. J.: Precise radiocarbon dating of the giant Weis landslide (Eastern Alps,
410 Austria), Geomorphology, 243, 87-91, 10.1016/j.geomorph.2016.05.001, 2015.
411 Nilaweera, N. S., and Nutalaya, P.: Role of tree roots in slope stabilisation, Bulletin of Engineering Geology & the
412 Environment, 57, 337-342, 1999.
413 Nourani, V., Pradhan, B., Ghaffari, H., and Sharifi, S. S.: Landslide susceptibility mapping at Zonouz Plain, Iran using
414 genetic programming and comparison with frequency ratio, logistic regression, and artificial neural network models, Nat
415 Hazards, 71, 523-547, 10.1007/s11069-013-0932-3, 2014.
416 Ocakoglu, F., Gokceoglu, C., and Ercanoglu, M.: Dynamics of a complex mass movement triggered by heavy rainfall: a case
417 study from NW Turkey, Geomorphology, 42, 329-341, Doi 10.1016/S0169-555x(01)00094-0, 2002.
418 Pasculli, A., Sciarra, N., Esposito, L., and Esposito, A. W.: Effects of wetting and drying cycles on mechanical properties of
419 pyroclastic soils, Catena, 156, 113-123, 10.1016/j.catena.2017.04.004, 2017.
420 Peng, J. B., Fan, Z. J., Wu, D., Zhuang, J. Q., Dai, F. C., Chen, W. W., and Zhao, C.: Heavy rainfall triggered
421 loess-mudstone landslide and subsequent debris flow in Tianshui, China, Eng Geol, 186, 79-90, 2015.
422 Persichillo, M. G., Bordoni, M., and Meisina, C.: The role of land use changes in the distribution of shallow landslides, Sci.
423 Total Environ., 574, 924-937, 10.1016/j.scitotenv.2016.09.125, 2017.
424 Peruccacci, S., Brunetti, M. T., Luciani, S., Vennari, C., and Guzzetti, F.: Lithological and seasonal control on rainfall
425 thresholds for the possible initiation of landslides in central Italy, Geomorphology, 139, 79-90,
426 10.1016/j.geomorph.2011.10.005, 2012.
427 Petley, D. N.: On the impact of climate change and population growth on the occurrence of fatal landslides in South, East
428 and SE Asia, Q J Eng Geol Hydroge, 43, 487-496, 10.1144/1470-9236/09-001, 2010.
429 Pradhan, B., and Youssef, A. M.: Manifestation of remote sensing data and GIS on landslide hazard analysis using
430 spatial-based statistical models, Arab J Geosci, 3, 319-326, 10.1007/s12517-009-0089-2, 2010.
431 Qin, S. Q., Jiao, J. J., and Wang, S. J.: The predictable time scale of landslides, Bulletin of Engineering Geology & the
432 Environment, 59, 307-312, 2001.
433 Saito, H., Korup, O., Uchida, T., Hayashi, S., and Oguchi, T.: Rainfall conditions, typhoon frequency, and contemporary
434 landslide erosion in Japan, Geology, 42, 999-1002, 2014.

435   Sorbino, G., Sica, C., and Cascini, L.: Susceptibility analysis of shallow landslides source areas using physically based
436   models, Nat Hazards, 53, 313-332, 10.1007/s11069-009-9431-y, 2010.
437   Sun, P., Peng, J. B., Chen, L. W., Lu, Q. Z., and Igwe, O.: An experimental study of the mechanical characteristics of
438   fractured loess in western China, B Eng Geol Environ, 75, 1639-1647, 10.1007/s10064-015-0793-y, 2016.
439   Turner, T. R., Duke, S. D., Fransen, B. R., Reiter, M. L., Kroll, A. J., Ward, J. W., Bach, J. L., Justice, T. E., and Bilby, R. E.:
440   Landslide densities associated with rainfall, stand age, and topography on forested landscapes, southwestern Washington,
441   USA, For. Ecol. Manage., 259, 2233-2247, 2010.
442   van Asch, T. W. J., and Malet, J. P.: Flow-type failures in fine-grained soils: an important aspect in landslide hazard analysis,
443   Nat Hazard Earth Sys, 9, 1703-1711, 10.5194/nhess-9-1703-2009, 2009.
444   Wooten, R. M., Gillon, K. A., Witt, A. C., Latham, R. S., Douglas, T. J., Bauer, J. B., Fuemmeler, S. J., and Lee, L. G.:
445   Geologic, geomorphic, and meteorological aspects of debris flows triggered by Hurricanes Frances and Ivan during
446   September 2004 in the Southern Appalachian Mountains of Macon County, North Carolina (southeastern USA), Landslides,
447   5, 31-44, 2008.
448   Wu, H., and Qian, H.: Innovative trend analysis of annual and seasonal rainfall and extreme values in Shaanxi, China, since
449   the 1950s, International Journal of Climatology, 37, 2582-2592, 10.1002/joc.4866, 2017.
450   Zezere, J. L., Vaz, T., Pereira, S., Oliveira, S. C., Marques, R., and Garcia, R. A. C.: Rainfall thresholds for landslide activity
451   in Portugal: a state of the art, Environ Earth Sci, 73, 2917-2936, 2015.
452   Zhang, K., Xue, X. W., Hong, Y., Gourley, J. J., Lu, N., Wan, Z. M., Hong, Z., and Wooten, R.: iCRESTRIGRS: a coupled
453   modeling system for cascading flood-landslide disaster forecasting, Hydrol. Earth Syst. Sci., 20, 5035-5048, 2016.
454   Zhang, P., Ma, J. Z., Shu, H. P., Han, T., and Zhang, Y. L.: Simulating debris flow deposition using a two-dimensional finite
455   model and Soil Conservation Service-curve number approach for Hanlin gully of southern Gansu (China), Environ Earth Sci,
456   73, 6417-6426, 2015.
457   Zhang, Y. C., Zhang, F., Zhang, J. Q., Guo, E. L., Liu, X. P., and Tong, Z. J.: Research on the Geological Disaster Forecast
458   and Early Warning Model Based on the Optimal Combination Weighing Law and Extension Method: a Case Study in China,
459   Pol J Environ Stud, 26, 2385-2395, 10.15244/pjoes/69100, 2017.
460   Zhou, J. W., Cui, P., Yang, X. G., Su, Z. M., and Guo, X. J.: Debris flows introduced in landslide deposits under rainfall
461   conditions: The case of Wenjiagou gully, J Mt Sci-Engl, 10, 249-260, 2013.
462   Zhu, X., Xu, Q., Tang, M. G., Nie, W., Ma, S. Q., and Xu, Z. P.: Comparison of two optimized machine learning models for
463   predicting displacement of rainfall-induced landslide: A case study in Sichuan Province, China, Eng Geol, 218, 213-222,
464   10.1016/j.enggeo.2017.01.022, 2017.
465   Zhuang, J. Q., and Peng, J. B.: A coupled slope cutting-a prolonged rainfall-induced loess landslide: a 17 October 2011 case
466   study, B Eng Geol Environ, 73, 997-1011, 2014.

467

468   **Figure Captions:**

469   **Figure 1: Spatial maps of (a) elevation, (b) land cover and (c) soil type across the study region.**

470   **Figure 2: Locations of reported rainfall-triggered landslide and debris flow events and the resultant casualties in Shaanxi Province**
471   **from 2009 to 2012; the inset shows the location of Shaanxi Province in China.**

472   **Figure 3: (a) Interannual distributions of reported landslide and debris flow events and the associated casualties from 2009 to**
473   **2012, and (b) pie charts of the disaster types and their corresponding casualties.**

474   **Figure 4: (a) Yearly distributions and (b) monthly distributions of rainfall amount, the number of landslide events, and the**
475   **number of debris flow events from 2009 to 2012, and (c) the distribution of multi-year mean monthly rainfall intensity.**

476   **Figure 5: Distributions of annual rainfall amount, landslide events, and debris flow events along the latitude bands, and spatial**
477   **average slopes and percentages of dominant land cover types in these latitude bands.**

478   **Figure 6: Relationship of occurrence rates of landslide and debris flow events with the corresponding (a) accumulated amount of**
479   **antecedent continuous rainfall, (b) rainfall duration, and (c) average rainfall intensity.**

480   **Figure 7: Regional average occurrence rates of landslide and debris flow events under different rainfall intensity classes.**

481   **Figure 8: Spatial distributions of the occurrence rates of (a-d) landslide and (e-h) debris flow under four rainfall intensity classes:**
482   **light rain, moderate rain, heavy rain, and violent rain; only these grid cells with recorded landslide or debris flow events were**
483   **analyzed and plotted in this figure.**

484   **Figure 9: Occurrence rates of landslide and debris flow under different degrees of terrain slopes.**

485   **Figure 10: Occurrence rates of landslide and debris flow under different (a) land cover types and (b) soil types.**

486

487   **Figure 1: Spatial maps of (a) elevation, (b) land cover and (c) soil type across the study region.**
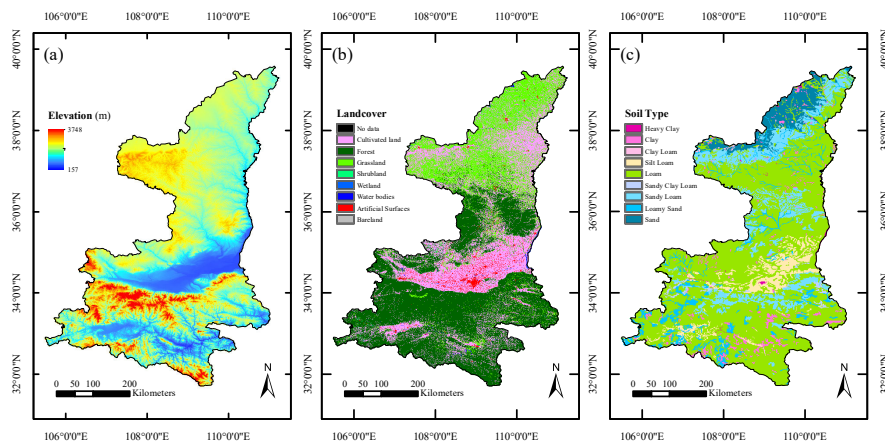
488

489

490   **Figure 2: Locations of reported rainfall-triggered landslide and debris flow events and the resultant casualties in Shaanxi Province**

491   **from 2009 to 2012; the inset shows the location of Shaanxi Province in China.**
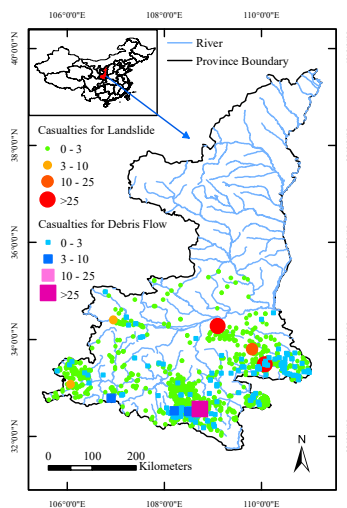
492

493

494 **Figure 3: (a) Interannual distributions of reported landslide and debris flow events and the associated casualties from 2009 to**

495 **2012, and (b) pie charts of the disaster types and their corresponding casualties.**
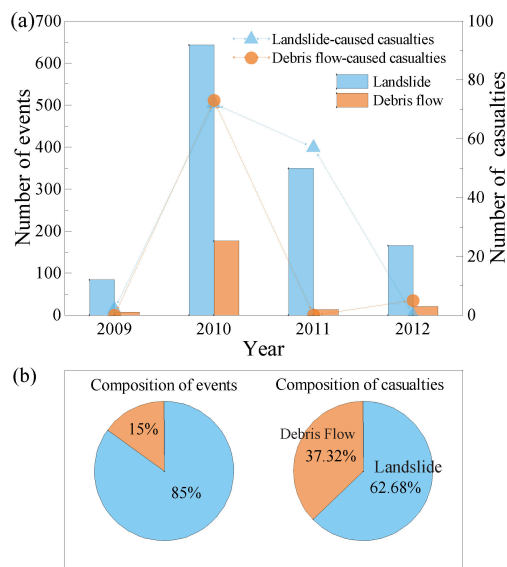
496

497

Figure 4: (a) Yearly distributions and (b) monthly distributions of rainfall amount, the number of landslide events, and the number of debris flow events from 2009 to 2012, and (c) the distribution of multi-year mean monthly rainfall intensity.
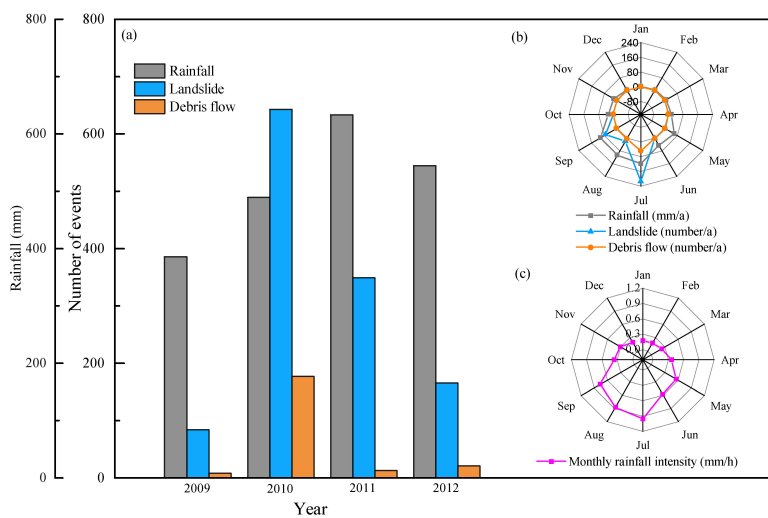
502   **Figure 5: Distributions of annual rainfall amount, landslide events, and debris flow events along the latitude bands, and spatial**

503   **average slopes and percentages of dominant land cover types in these latitude bands.**
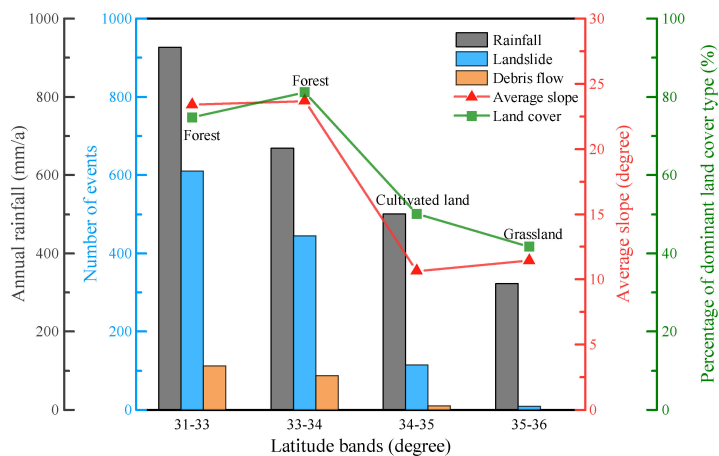
504

505

506 **Figure 6: Relationship of occurrence rates of landslide and debris flow events with the corresponding (a) accumulated amount of**

507 **antecedent continuous rainfall, (b) rainfall duration, and (c) average rainfall intensity.**
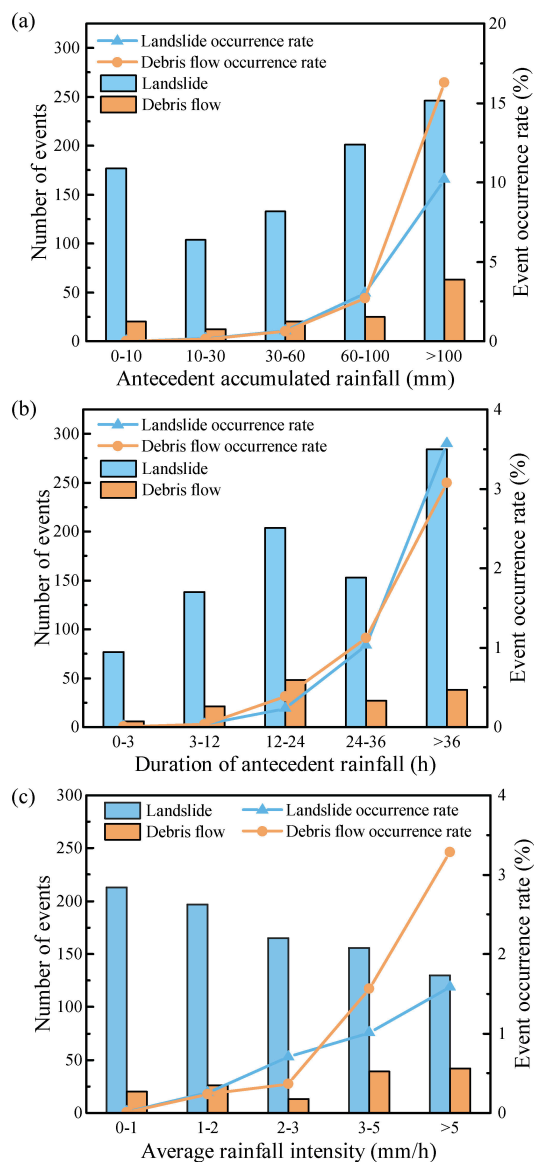
508

509

510

511 **Figure 7: Regional average occurrence rates of landslide and debris flow events under different rainfall intensity classes.**
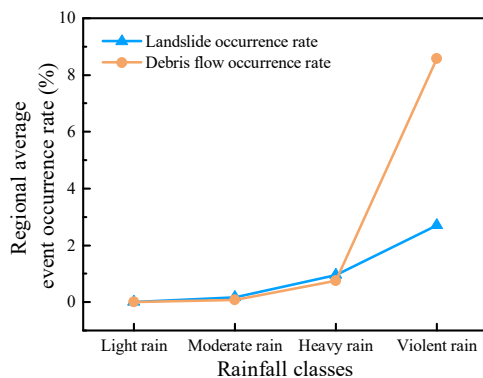
512

513

514   **Figure 8: Spatial distributions of the occurrence rates of (a-d) landslide and (e-h) debris flow under four rainfall intensity classes:**

515   **light rain, moderate rain, heavy rain, and violent rain; only these grid cells with recorded landslide or debris flow events were**

516   **analyzed and plotted in this figure.**
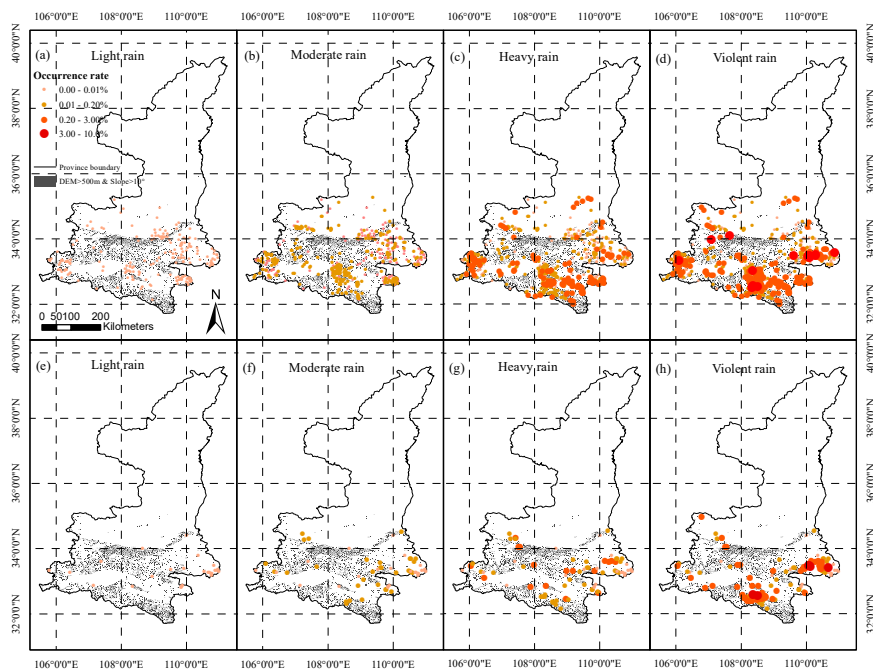
517

518

519   **Figure 9: Occurrence rates of landslide and debris flow under different degrees of terrain slopes.**
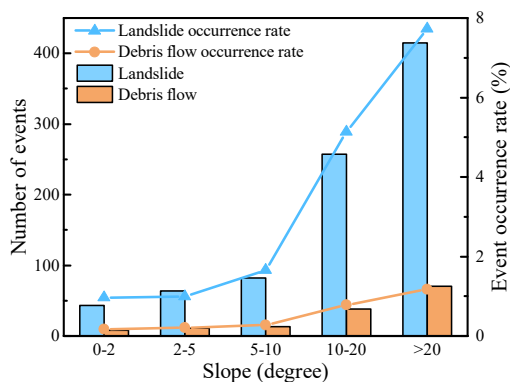
520

521   **Figure 10: Occurrence rates of landslide and debris flow under different (a) land cover types and (b) soil types.**

522

523